Reduced-Order Model for Supersonic Transport Takeoff Noise Scaling with Cruise Mach Number

Laurens J. A. Voet,* Prakash Prashanth,† Raymond L. Speth,‡ Jayant S. Sabnis,§ Choon S. Tan,¶ and Steven R. H. Barrett**
Massachusetts Institute of Technology, Cambridge, Massachusetts 02139

https://doi.org/10.2514/1.C037633

The recent interest in the development of supersonic transport raises concerns about an increase in community noise around airports. As noise certification standards for supersonic transport other than Concorde have not yet been developed by the International Civil Aviation Organization, there is a need for a physics-based scaling rule for supersonic transport takeoff noise performance. Assuming supersonic transport takeoff noise levels are dominated by the engine mixed jet velocity and the aircraft-to-microphone propagation distance, this paper presents a reduced-order model for supersonic transport takeoff noise levels as a function of four scaling groups: cruise Mach number, takeoff aerodynamic efficiency, takeoff speed, and number of installed engines. This paper finds that, as cruise Mach number increases, supersonic transport takeoff noise levels increase while their thrust cutback noise reduction potential decreases. Assuming constant aerodynamic efficiency, takeoff speed, and number of installed engines, the takeoff noise levels and noise reduction potential of a Mach 2.2 aircraft are found to be ∼15.3 dB higher and ∼19.2 dB less compared to a Mach 1.4 aircraft, respectively. This scaling rule can potentially yield a simple guideline for estimating an approximate noise limit for supersonic transport, depending on their cruise Mach number.

Nomenclature

a_0	=	ambient speed of sound, m/s
c_L, c_D	=	aircraft lift and drag coefficient
$EPNL$	=	effective perceived noise level, EPNdB
F_n	=	engine net thrust, N
$f(\cdot)$	=	functional form of $(\cdot)$
g	=	gravitational acceleration, $\mathrm{m/s^2}$
k_{TO}	=	ratio of takeoff to stall speed
L, D	=	aircraft lift and drag force, N
M_{cruise}	=	cruise Mach number
m	=	aircraft mass, kg
N_e	=	number of installed engines
P	=	noise power level, dB
p_0	=	ambient pressure, Pa
r	=	propagation distance, m
V	=	aircraft velocity, m/s
V_j	=	engine mixed jet velocity, m/s
W	=	aircraft weight, N
x	=	distance past brake release, m
y	=	lateral distance from takeoff centerline, m
z	=	altitude, m
α	=	aircraft angle of attack, deg
γ	=	aircraft climb angle, deg
Λ	=	aircraft aerodynamic efficiency, L/D
λ	=	engine thrust lapse
Π	=	noise power, W
ρ_0	=	ambient density, $\mathrm{kg/m^3}$
τ	=	engine thrust setting
ψ	=	thrust loading, F_n/W
ω	=	aircraft wing loading, $\mathrm{N/m^2}$

I. Introduction

THERE has been a recent interest in the development of supersonic transport (SST), which raises concerns about an increase in noise around airports, given the noise levels of Concorde in comparison to subsonic aviation at the time [1,2]. Standards and Recommended Practices (SARPs) for noise certification of supersonic aircraft other than Concorde have not yet been developed by the International Civil Aviation Organization (ICAO). Currently, the SARPs for subsonic jet aircraft are recommended to be used as guidance [3]. Extrapolating the noise performance from Concorde —an SST vehicle developed more than 50 years ago and out-of-service for almost 20 years—for developing noise SARPs for the next-generation civil SST is clearly an unsatisfactory proposition. Likewise, extrapolating noise certification trends from existing subsonic aircraft is similarly an insufficient proposition, as SST aircraft are significantly different from subsonic aircraft in terms of their airframe and engine design, as well as their operation.

In an effort to set noise certification SARPs for the next-generation SST, the Federal Aviation Administration (FAA) published a Notice for Proposed Rule Making (NPRM) in April 2020 on Noise Certification of Supersonic Airplanes [4]. In this NPRM, they suggested a new noise category—the Supersonic Level 1 (SSL1) aircraft class—for SST limited to a maximum takeoff weight of 68,039 kg (150,000 lbm), a maximum number of three installed engines, and a maximum operating Mach number of 1.8. Further, they proposed noise stringency levels for the SSL1-type aircraft between ICAO Annex 16, Volume I, Chapter 4 and Chapter 14 levels [3]. Similar to FAA, the European Union Aviation Safety Agency (EASA) proposed noise certification standards for all SST airplanes in their Advance Notice for Proposed Amendment (A-NPA) of May 2022 [5]. EASA suggested stringency levels equal to those for subsonic transport in Annex 16, Chapter 14. Recently, the United States also declared their support of the development of supersonic LTO noise standards based on Annex 16, Chapter 14, limits for commercial subsonic transport [6].

For the first time in history, the aircraft noise standards proposed by FAA and EASA are based solely on noise model calculations rather than on noise measurements [4,5,7]. Furthermore, the SSL1-type aircraft class does not span the entire range of possible SSTs currently

Presented as Paper 2023-3725 at the AIAA Aviation 2023 Forum, San Diego, CA, June 12–16, 2023; received 29 July 2023; revision received 10 January 2024; accepted for publication 17 February 2024; published online Open Access 2 April 2024.

*Independent Researcher; laurens.ja.voet@gmail.com. Member AIAA (Corresponding Author).
†Research Scientist, Department of Aeronautics and Astronautics. Member AIAA.
‡Principal Research Scientist, Department of Aeronautics and Astronautics.
§Senior Lecturer, Department of Aeronautics and Astronautics. Fellow AIAA.
¶Senior Research Engineer, Department of Aeronautics and Astronautics. Senior Member AIAA.
**Professor, Department of Aeronautics and Astronautics. Senior Member AIAA.

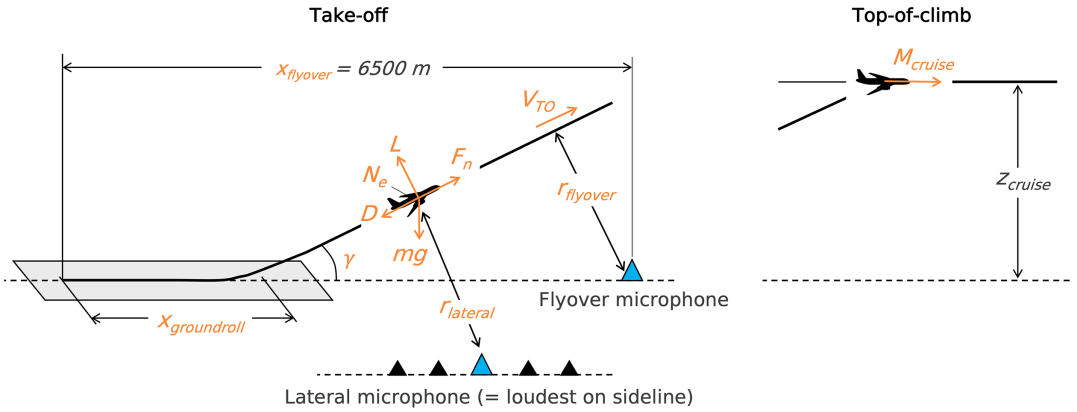

Fig. 1 Relevant variables for aircraft takeoff performance for noise assessments. Left: takeoff; right: top-of-climb as airframe aerodynamic design point and engine sizing point.

being developed by industry [4]. To the best of the authors' knowledge, no previous work has formulated a reduced-order model to scale SST takeoff noise levels for different size classes and cruise Mach numbers. Such a scaling rule can potentially yield a simple guideline for regulatory authorities to estimate approximate noise limits for SST depending on their cruise Mach number. Furthermore, it can enable the impact assessment of key vehicle design parameters on the takeoff noise performance of SST, which could be used in trade studies with other vehicle performance metrics.

The reduced-order model for SST takeoff noise scaling is informed by three disciplines: a) propulsion system thermodynamic cycle models developed using the Numerical Propulsion System Simulation (NPSS) software [8] to describe the engine design and thus the source noise characteristics; b) trajectory models developed using the NASA Dymos package [9] within NASA OpenMDAO [10] to describe the dynamics of the aircraft operations during takeoff and the propagation characteristics; and c) takeoff noise data computed using the Python Noise Assessment (pyNA) tool [11] to anchor the reduced-order model.

A *standard* takeoff trajectory abiding by the noise certification standards for subsonic transport is employed in the reduced-order model. The aircraft takes off at 100% thrust until the allowable cutback altitude is reached.[††] Subsequently, the pilot cuts back the thrust not below the level required to maintain a 4% climb gradient or steady level flight with one engine inoperative (OEI), whichever thrust is greater [3]. The aircraft velocity during takeoff shall be between $V_2 + 5.1$ m/s (10 kts) and $V_2 + 10.2$ m/s (20 kts), where V_2 is the takeoff safety speed. It is of interest to scale the takeoff noise (i.e., the sum of lateral and flyover noise) as well as the noise reduction potential of the pilot-initiated thrust cutback procedure for SST of different size classes and cruise Mach numbers. Modified takeoff procedures have been proposed in the literature [1,12–14], as well as the regulatory SARPs proposals by FAA and EASA [4,5] for SST takeoff noise reduction. Such procedures are enabled by variable noise reduction systems (VNRS), defined as dynamic systems integrated into the aircraft design functioning automatically to change the engine operation or airframe configuration to reduce noise [15], e.g., programmed thrust cutback [16,17]. To avoid dealing with the large range of possible VNRS, the reduced-order model is evaluated at the *lower limit for the takeoff noise levels* of SST with VNRS.

The ICAO certification noise framework [3] is a surrogate measure of noise exposure around the airport, measuring effective perceived noise level (EPNL) at three predefined microphones around the approach and takeoff trajectory. Even though noise metrics like sound exposure level or day–night average sound level could better capture the community noise nuisance around airports, they are not scalar values that can readily be compared or optimized as they have high spatial dependence and thus are not used in this work. This reduced-order model presented in this paper estimates takeoff noise levels, defined as the sum of flyover and lateral noise, based on two microphone locations: flyover noise is measured at the *flyover* microphone, which is fixed underneath the flight path at 6500 m past the brake release point; lateral noise is measured at the *lateral* microphone, defined as the loudest microphone on the 450 m sideline [3]. Because the reduced-order model uses the ICAO noise certification framework as a surrogate measure of noise exposure, there is a need to assess the impact of any derived noise limits on the community noise around the airport, which is considered beyond the scope of this paper.

This paper is outlined as follows: Section II presents an expression for the microphone noise level from the propagation effects of a compact noise source strength. Four relevant scaling groups for the microphone noise levels of SST takeoff trajectories are identified in Sec. III. The reduced-order model formulation is outlined in Sec. IV. The utility of the reduced-order model is assessed in Sec. V by estimating the takeoff noise levels of a supersonic business jet and an airliner: the Supersonic Technology Concept Airplane (STCA) [18] developed by NASA and the Georgia Institute of Technology (GT) Medium SST [19], respectively. Finally, the reduced-order model is applied to assess the takeoff noise performance of a broad class of supersonic vehicles.

II. Microphone Noise Levels by Propagating Compact Noise Source Strength

The lateral and flyover microphones of the ICAO noise certification framework are illustrated in Fig. 1. The noise level measured at a microphone, $P_{\text{microphone}}$, is determined by first estimating the noise source power and then applying the propagation effects between the source and the microphone as the acoustic waves pass through the atmosphere. The noise power Π_{source} is defined with respect to human hearing threshold power $\Pi_{\text{ref}} = 1 \cdot 10^{-12}$ (W/m^2)[‡‡]:

$$P_{\text{microphone}} = 10\log_{10}\left[\frac{\Pi_{\text{source}}}{\Pi_{\text{ref}}} \cdot \Pi_{\text{propagation}}\right] = 10\log_{10}\left[\frac{\Pi_{\text{source}}}{\Pi_{\text{ref}}}\right] + 10\log_{10}[\Pi_{\text{propagation}}] \quad (1)$$

The noise source power Π_{source} and propagation effects $\Pi_{\text{propagation}}$ are approximated by the dominant (zeroth-order) terms. To account for these approximations, it is necessary to introduce two correlating proportionality constants (c_1 and c_2) when estimating the noise level at the microphone using Eq. (1). The noise level at the microphone is thus given by

$$P_{\text{microphone}} = c_1 P_{\text{source}} + c_2 P_{\text{propagation}} \quad (2)$$

[††]The allowable cutback altitude is defined as 260 m (853 ft) for a three-engine aircraft and as 210 m (689 ft) for a four-engine aircraft [3].

[‡‡]Alternatively, $P_{\text{microphone}}$ can be cast as acoustic power normalized by the jet mechanical (kinetic) power.

The approximations for the source level term P_{source} and for the propagation effects term $P_{\text{propagation}}$ are given in decibels. The coefficients c_1 and c_2 of the linear combination are determined using a least-square fit with noise data at a flyover microphone, as outlined in Sec. IV.C.

Sections II.A and II.B approximate the noise source strength P_{source} and the noise propagation effects P_{observer} by identifying their respective drivers. The reduced-order model aims to capture the first-order governing effects to estimate the trends of the SST takeoff noise levels with key scaling variables, rather than to compute takeoff noise levels with high-fidelity.

A. Noise Source Strength, P_{source}

SST takeoff noise levels are dominated by the jet mixing source [18]. The SST noise source strength is thus approximated using Lighthill's eighth power law [20] for aerodynamic sound generation:

$$P_{\text{source}} = 10\log_{10}\left(\frac{K\frac{\rho_0}{c_0^5}L^2U^8}{\Pi_{\text{ref}}}\right) \sim 10\log_{10}(U)^8 \tag{3}$$

In Eq. (3), P_{source} is the far-field source acoustic power in decibels, K is Lighthill's constant, L is the characteristic length scale of the sound source, U is the characteristic velocity scale of the sound source, and ρ_0 and c_0 are the ambient density and speed of sound, respectively. Equation (3) is an expression for the acoustic power and does not capture frequency effects, including the Doppler and convective amplification. The dominant velocity term in Eq. (3) (U^8) is retained for the source strength, i.e., $P_{\text{source}} \sim 10\log_{10}(U)^8$. For high-speed jets with $M_{\text{jet}} \geq 2$, $P_{\text{source}} \sim 10\log_{10}(U)^3$. The characteristic velocity scale for Lighthill's eighth power law is the shear between the jet and the ambient, i.e., the difference between the engine mixed jet and ambient velocity ($U = V_j - V_{\text{TO}}$). The engine mixed jet velocity V_j is decomposed into two terms to represent the effects of engine design and engine operation:

$$V_j = \underbrace{V_{j,\tau=1}}_{\text{Engine design}} \underbrace{-\frac{\partial V_j}{\partial \tau}(1-\tau_{\text{cutback}})}_{\text{Engine operation}} \tag{4}$$

The engine thrust setting τ in Eq. (4) is defined as the ratio of net thrust at a flight condition and the maximum thermodynamically available thrust at that flight condition at 100% high-pressure spool speed. The first term $V_{j,\tau=1}$ denotes the mixed jet velocity when the engine is operated at 100% available thrust, i.e., $\tau = 1$; the second term denotes the decrease in mixed jet velocity because of a thrust cutback τ_{cutback}. The engine noise source strength is thus given by

$$P_{\text{source}} \sim 10\log_{10}\left[\left(V_{j,\tau=1} - \frac{\partial V_j}{\partial \tau}(1-\tau_{\text{cutback}})\right) - V_{\text{TO}}\right]^8 \tag{5}$$

B. Noise Propagation Effects, $P_{\text{propagation}}$

The noise propagation effects between the source and microphone are spherical spreading, atmospheric absorption, characteristic impedance ratio correction, ground attenuation and reflection effects, as well as lateral attenuation effects. The spherical spreading effect is the dominant term; the other effects are thus neglected so that the propagation effects are determined from:

$$P_{\text{propagation}} \sim 10\log_{10}\left(\frac{1}{r}\right)^2 \tag{6}$$

The propagation distance r between the source and microphone is a function of the (moving) source position and, thus, a function of time. The EPNL is a time-integrated noise metric, i.e., a single value for characterizing the noise at a microphone for a noise source (aircraft) along a trajectory. Thus, the minimum distance between the noise source and the microphone, r_{min}, is chosen as representative metric for the propagation effects:

$$P_{\text{propagation}} \sim 10\log_{10}\left(\frac{1}{r_{\text{min}}}\right)^2 \tag{7}$$

The minimum propagation distance for the lateral and flyover microphone is denoted by r_{lateral} and r_{flyover}, respectively.

III. Relevant SST Vehicle and Mission Scaling Groups

The Buckingham-Π theorem provides a framework to determine sets of dimensionless parameters to characterize a physical phenomenon. This approach is used to obtain the relevant vehicle and mission scaling groups for the noise source strength and the propagation effects. Figure 1 shows the takeoff and top-of-climb operating points for an SST, including the relevant physical variables associated with the aircraft takeoff noise performance. Table 1 lists these variables and their respective units, as well as computes the corresponding Π groups.

A. Noise Source Strength, P_{source}

Engines designed for SST are sized at mission top-of-climb as most demanding operating point. The required aircraft thrust loading $F_{\text{n,req.}}/W$ at this operating point is derived from the equations of motion of climbing flight:

$$\left.\frac{F_{\text{n,req.}}}{W}\right|_{\text{TOC}} = \left[\frac{1}{\Lambda_{\text{TOC}}} + \frac{V_z}{V_{\text{cruise}}}\right] \tag{8}$$

where V_z denotes the rate of climb. Using the definition of engine net thrust, $F_{\text{n,engine}} = \dot{m}_{\text{engine}}(V_j - V_0)$, Eq. (8) is re-arranged to obtain the engine specific thrust at mission top-of-climb:

$$(V_j - V_0)|_{\text{TOC}} = \left[\frac{W}{\dot{m}_{\text{engine}}N_e}\right]\left[\frac{1}{\Lambda_{\text{TOC}}} + \frac{V_z}{V_{\text{cruise}}}\right] = f(M_{\text{cruise}}) \tag{9}$$

The ratio $[W/(\dot{m}_{\text{engine}}N_e)]$ is assumed to only be a function of cruise Mach number; i.e., changes in aircraft maximum takeoff weight and number of installed engines are counterbalanced by changes in engine mass flow without changing the engine specific thrust. Because of this assumption, the reduced-order model does not depend on aircraft maximum takeoff weight or cruise range. The aerodynamic efficiency at top-of-climb, Λ_{TOC}, is assumed to be

Table 1 Buckingham-Π theorem applied to aircraft takeoff performance: 16 variables and 3 dimensions (length L, mass M, and time T) resulting in 13 independent Π groups

No.	Variable	Unit	Π group
1	P_{source}	— —	P_{source}
2	P_{lateral}	— —	P_{lateral}
3	P_{flyover}	— —	P_{flyover}
4	M_{cruise}	— —	M_{cruise}
5	$x_{\text{groundroll}}$	L	$\frac{x_{\text{groundroll}}}{x_{\text{flyover}}}$
6	r_{lateral}	L	$\frac{r_{\text{lateral}}}{x_{\text{flyover}}}$
7	r_{flyover}	L	$\frac{r_{\text{flyover}}}{x_{\text{flyover}}}$
8	γ	— —	γ
9	L	$\frac{ML}{T^2}$	$\frac{L}{mg}$
10	D	$\frac{ML}{T^2}$	$\frac{D}{mg}$
11	F_n	$\frac{ML}{T^2}$	$\frac{F_n}{mg}$
12	V_{TO}	$\frac{L}{T}$	$\frac{V_{\text{TO}}^2}{x_{\text{flyover}}g}$
13	N_e	— —	N_e
14	x_{flyover}	L	— —
15	m	M	— —
16	g	$\frac{L}{T^2}$	— —

proportional to the cruise Mach number. Küchemann [21] presents an aerodynamic efficiency target, $\Lambda_{\text{TOC}} = 3((M_{\text{cruise}} + 3)/M_{\text{cruise}})$, for SST across cruise Mach numbers. The potential rate-of-climb requirement at top-of-climb, V_z, is assumed to be constant, equal to 4.11 m/s (810 ft/min), for all vehicles in the design space, based on the NASA STCA mission profile [18]. Finally, the cruise altitude of SST cruise is within the (isothermal) stratosphere, where the cruise velocity is given by $V_{\text{cruise}} = a_{\text{cruise}} M_{\text{cruise}}$. The engine specific thrust at top-of-climb in Eq. (9) is thus solely a function of cruise Mach number.

In the engine design process, the designer first decides the engine thermodynamic cycle, which sets the engine specific thrust. Subsequently, the engine is physically *sized* to meet the aircraft thrust requirements; i.e., the engine mass flow requirement is determined. By establishing that the specific thrust at top-of-climb is solely a function of the cruise Mach number [Eq. (9)], it is assumed that the engine thermodynamic cycle is thus simply set by the cruise Mach number. Furthermore, the relationship between the design and off-design points—between top-of-climb and the sea-level takeoff—is also governed by the thermodynamic cycle and thus also by the cruise Mach number. Therefore, it is reasoned that the specific thrust at the sea-level takeoff operating condition is also simply a function of the cruise Mach number. The engine jet velocity at sea-level takeoff, governing the noise source strength [see Eq. (5)], can be readily derived from the engine specific thrust and thus is also governed solely by the cruise Mach number. This result is significant as it shows that, to assess the source noise of SST, the engine design space is thus reduced to a single scaling group, $\Pi_1 = M_{\text{cruise}}$. Similarly, the rate of the engine mixed jet velocity with thrust setting is also solely a function of the cruise Mach number.

The minimum allowable cutback thrust setting is defined as the ratio of required to available net thrust at takeoff. The available thrust loading at takeoff is assumed to solely be a function of the cruise Mach number M_{cruise}. The required thrust is governed by the steady level flight with one-engine-inoperative requirement and is thus a function of the takeoff aerodynamic efficiency and number of installed engines, N_e [see Eq. (8)]. Note that the aircraft aerodynamic efficiency is also a function of takeoff speed, i.e., $(\Pi_9/\Pi_{10}) = f(\Pi_{12})$. In this paper, the aerodynamic efficiency at a given (takeoff) velocity is assumed to be a technology-level characteristic Λ_{TO} and thus a constant for a given aircraft. It is assumed that the aerodynamic efficiency scales with the takeoff speed squared.[§§] The noise source strength P_{source} is thus given by

$$P_{\text{source}} = \Pi_1 = f\left(\Pi_4 = M_{\text{cruise}}, \frac{\Pi_9}{\Pi_{10}} = \Lambda_{\text{TO}}, \Pi_{12} = \frac{V_{\text{TO}}^2}{x_{\text{flyover}} g}, \Pi_{13} = N_e\right) \tag{10}$$

B. Noise Propagation Effects, $P_{\text{propagation}}$

1. Lateral Propagation Distance

It is assumed that the lateral microphone is located on the sideline ($y = 450$ m) at the point where the aircraft reaches 300 m (985 ft) altitude. This assumption is referenced in the equivalent noise certification procedures for jet airplanes in 14 CFR §B26.3(a)(1) [22]. This results in a fixed lateral microphone propagation distance for various vehicles:

$$\frac{r_{\text{lateral}}}{x_{\text{flyover}}} = \Pi_2 = \text{constant} = \frac{\sqrt{450^2 + 300^2}\ [\text{m}]}{6500\ [\text{m}]} = 0.08 \tag{11}$$

[§§]The aerodynamic efficiency is given by $\Lambda = (c_L/c_{D,0} + k_0 c_L^2) \sim (1/c_L) \sim V^2$, where $c_{D,0}$ is the zero-lift drag coefficient and k_0 is the inverse of the product of the constant π, the wing aspect ratio, AR, and the Oswald efficiency factor, e, i.e. $k_0 = 1/\pi \cdot AR \cdot e$. The drag term in the denominator is dominated by the induced drag for delta wings at high angles of attack during takeoff conditions.

2. Flyover Propagation Distance

The flyover propagation distance is computed using geometry from the groundroll distance $x_{\text{groundroll}}$ and the climb angle γ (see Fig. 1), i.e., $\Pi_7 = f(\Pi_5, \Pi_8)$. During the groundroll, the aircraft accelerates from standstill to takeoff speed V_{TO} by applying thrust F_n. As stated above, the available thrust at takeoff is a function of the cruise Mach number M_{cruise}. Thus, the groundroll distance $\Pi_5 = f(\Pi_4, \Pi_{12})$. The aircraft climb angle is obtained from the equations of steady climbing flight:

$$\gamma = \sin^{-1}\left(\psi_{\text{TO}} - \frac{1}{\Lambda_{\text{TO}}}\right) \tag{12}$$

Thus, the climb angle $\Pi_8 = f(\Pi_4, (\Pi_9/\Pi_{10}))$. Finally, the flyover propagation distance is written as

$$\frac{r_{\text{flyover}}}{x_{\text{flyover}}} = \Pi_3 = f\left(\Pi_4 = M_{\text{cruise}}, \frac{\Pi_9}{\Pi_{10}} = \Lambda_{\text{TO}}, \Pi_{12} = \frac{V_{\text{TO}}^2}{x_{\text{flyover}} g}\right) \tag{13}$$

C. Microphone Noise Levels, $P_{\text{microphone}}$

To conclude, by combining Eqs. (10), (11), and (13), the SST takeoff noise levels at the lateral and flyover microphone are written in terms of four scaling groups:

$$P_{\text{lateral}}, P_{\text{flyover}} = \Pi_2, \Pi_3 = f\left(\Pi_4 = M_{\text{cruise}}, \frac{\Pi_9}{\Pi_{10}} = \Lambda_{\text{TO}}, \Pi_{12} = \frac{V_{\text{TO}}^2}{x_{\text{flyover}} g}, \Pi_{13} = N_e\right) \tag{14}$$

The method to obtain the functional form f in Eq. (14) is described in Sec. IV.A.

IV. Reduced-Order Model Formulation

A. Noise Source Strength Parameters, $V_{\text{j},\tau=1}$, $\partial V_{\text{j}}/\partial\tau$, and τ_{cutback}

The SST engine design space is explored to formulate the expression [Eq. (10)] of the noise source strength parameters $V_{j,\tau=1}$, $(\partial V_j/\partial\tau)$, and τ_{cutback} as a function of the scaling groups identified in Sec. III. As shown in Sec. III.A., the engine source strength characteristics are a function of the cruise Mach number. A set of (clean-sheet) SST engines is designed within the range $M_{\text{cruise}} \in [1.4, 2.2]$ using the NPSS software [8]. Details of the engine architecture and design are presented in Appendix A. The engine performance characteristics—evaluated at four operating conditions (top-of-climb, cruise, sea-level takeoff, and sea-level static)—are used to formulate a reduced-order model for the noise source strength parameters, as outlined in the sections below.

1. Takeoff Jet Velocity at 100% Thrust Setting, $V_{\text{j},\tau=1}$

Figure 2a shows the specific thrust at the top-of-climb and sea-level takeoff operating points as a function of cruise Mach number from the NPSS cycle deck. A second-order polynomial regression of the sea-level takeoff specific thrust is computed using the performance data of the engines designed in NPSS, i.e., $V_{j,\tau=1} - V_{\text{TO}} = f(M_{\text{cruise}}, a, b, c)$. The takeoff condition in the NPSS cycle deck is computed at Mach 0.25, and thus $V_{\text{TO}} = 0.25 \cdot 340.3 = 85.1$ m/s. No operational part-power takeoff procedures are considered in this paper, which could be an additional degree of freedom for noise reduction of SST [12,23]. The takeoff jet velocity at 100% thrust setting is thus given by

$$V_{j,\tau=1} = aM_{\text{cruise}}^2 + bM_{\text{cruise}} + c\left[\frac{\text{m}}{\text{s}}\right] \quad \text{with} \begin{cases} a = +49.9 \\ b = -117.3 \\ c = +482.4 \end{cases} \tag{15}$$

As the cruise Mach number and, thus, the ram pressure ratio increase, lower compressor pressure ratios are required to meet the compressor

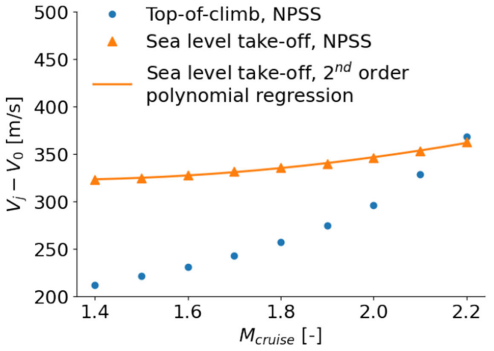

a) Specific thrust, $V_j - V_{TO}$

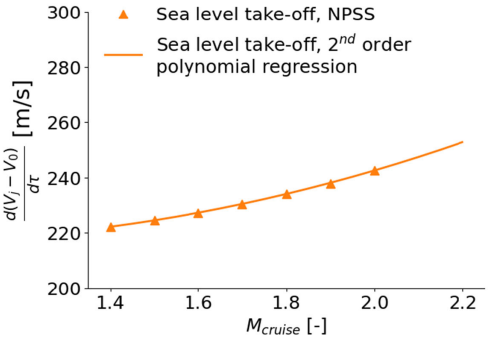

b) Rate of specific thrust, $V_j - V_{TO}$, with thrust setting, τ

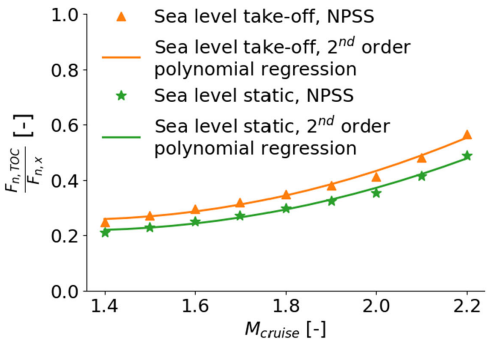

c) Thrust lapse, λ

Fig. 2 NPSS engine performance data (dots) as a function of cruise Mach number, $M_{\text{cruise}} \in [1.4, 2.2]$; second-order polynomial regression through performance data (solid line).

discharge pressure limit. For a fixed turbine inlet temperature limit, the enthalpy downstream of the low-pressure turbine thereby increases. Upon mixing with the fan stream, this higher-enthalpy gas is expanded through the nozzle, resulting in a higher jet velocity. Thus, the engine specific thrust at the top-of-climb (i.e., the engine sizing point) increases as the cruise Mach number increases. At the takeoff operating point, the increased specific thrust engine therefore also causes increased jet velocities, as shown in Fig. 2a.

2. *Rate of Change of Takeoff Jet Velocity with Thrust Setting, $\partial V_j/\partial\tau$*

Changes in the engine thrust setting τ cause changes in the engine jet velocity, characterized by the partial derivative $(\partial V_j/\partial\tau)$. The specific thrust is evaluated for the design sweep of engines at the sea-level takeoff operating point for a range of thrust settings, $\tau \in [0.5, 1.0]$. The rate of change of specific thrust with engine thrust setting is shown in Fig. 2b. As the cruise Mach number is increased, the specific thrust of the engines increases, meaning that the engines use less mass flow per unit thrust produced. When reducing the engine thrust, higher specific thrust engines will thus have a larger reduction in jet velocity.

A second-order polynomial regression of the rate of change of sea-level takeoff specific thrust with engine thrust setting is computed using the performance data of the engines designed in NPSS, i.e., $[(\partial(V_j - V_0))/\partial\tau] = (\partial V_j/\partial\tau) = f(M_{\text{cruise}}, a, b, c)$. Note that the partial derivative $(\partial V_{0,\text{TO}}/\partial\tau) = 0$. The rate of change of takeoff jet velocity with engine thrust setting is thus given by

$$\frac{\partial V_j}{\partial\tau} = aM_{\text{cruise}}^2 + bM_{\text{cruise}} + c\left[\frac{\text{m}}{\text{s}}\right] \quad \text{with} \quad \begin{cases} a = +21.5 \\ b = -39.2 \\ c = +234.8 \end{cases} \tag{16}$$

3. *Minimum Cutback Thrust Setting, τ_{cutback}*

The minimum allowable cutback thrust setting is defined as the ratio of required to available net thrust at takeoff. Since the mission top-of-climb sets the engine size as most demanding operating point, the required net thrust at top-of-climb equals the available net thrust, i.e., $F_{\text{n,avail.}}|_{\text{TOC}} = F_{\text{n,req.}}|_{\text{TOC}}$. The cutback thrust setting is thus given by

$$\tau_{\text{cutback}} = \underbrace{\left(\frac{\frac{F_{\text{n,req.}}}{W}\Big|_{\text{TO}}}{\frac{F_{\text{n,req.}}}{W}\Big|_{\text{TOC}}}\right)}_{\substack{\text{Ratio of required thrust loading} \\ \text{at takeoff and top-of-climb}}} \cdot \underbrace{\left(\frac{W_{\text{TO}}}{W_{\text{TOC}}}\right)}_{\substack{\text{Ratio of weight between} \\ \text{takeoff and top-of-climb}}} \cdot \underbrace{\left(\frac{F_{\text{n,avail.}}|_{\text{TOC}}}{F_{\text{n,avail.}}|_{\text{TO}}}\right)}_{\substack{\text{Thrust lapse between} \\ \text{top-of-climb and takeoff}}} \tag{17}$$

The three terms in Eq. (17) can be further rewritten as a function of cruise Mach number M_{cruise}, number of installed engines, N_e, and takeoff aerodynamic efficiency Λ_{TO}:

1) The required thrust loading for steady level flight ($V_z = 0$) at one-engine-inoperative ($N_e - 1$) is given by

$$\psi_{\text{TO}} = \frac{F_{\text{n,req.}}}{W}\bigg|_{\text{TO}} = \frac{1}{N_e - 1}\left[\frac{1}{\Lambda_{\text{TO}}}\right] \tag{18}$$

The required thrust loading at top-of-climb is given by

$$\begin{aligned} \psi_{\text{TOC}} &= \frac{F_{\text{n,req.}}}{W}\bigg|_{\text{TOC}} = \frac{1}{N_e}\left[\frac{1}{\Lambda_{\text{TOC}}} + \frac{V_z}{V_{\text{cruise}}}\right] \\ &= \frac{1}{N_e}\left[\frac{M_{\text{cruise}}}{3(M_{\text{cruise}} + 3)} + \frac{4.11}{295M_{\text{cruise}}}\right] \end{aligned} \tag{19}$$

2) The weight fraction between mission top-of-climb and takeoff is governed by the fuel burn between the two mission segments. Empirical data can be used to estimate mission segment fuel fractions during the preliminary design stage of a new vehicle. Nicolai and Carichner [24] present an empirical second-order polynomial regression of the weight fraction to climb and accelerate from takeoff to top-of-climb as a function of the cruise Mach number, i.e., $(W_{\text{TOC}}/W_{\text{TO}}) = f(M_{\text{cruise}}, a, b, c)$:

$$\frac{W_{\mathrm{TOC}}}{W_{\mathrm{TO}}} = aM_{\mathrm{cruise}}^2 + bM_{\mathrm{cruise}} + c \quad \text{with} \begin{cases} a = -0.0054 \\ b = -0.0357 \\ c = +1 \end{cases} \tag{20}$$

The second-order dependence of the weight fraction ($W_{\mathrm{TOC}}/W_{\mathrm{TO}}$) on the cruise Mach number can be explained from an energy perspective. During the path from takeoff to top-of-climb, fuel energy is converted into both potential energy ($\Delta PE = \rho_0 g z_{\mathrm{cruise}}$) and kinetic energy ($\Delta KE = (1/2)mV_{\mathrm{cruise}}^2 = (1/2)ma_0^2 M_{\mathrm{cruise}}^2$). Cruise altitude z_{cruise} is a function of cruise Mach number assuming cruise at constant dynamic pressure ($(1/2)p_0\gamma M_{\mathrm{cruise}}^2$). The fuel weight lost during the climb is thus proportional to the square of the cruise Mach number. The coefficients a, b, and c are set by the aircraft weight as well as aircraft design parameters that determine the cruise altitude (e.g., aircraft aerodynamics, wing area).

3) The thrust lapse λ is defined as the ratio of available thrust between top-of-climb—the engine sizing point—and any off-design operating points. Thrust lapse is the natural decrease in engine thrust with altitude and speed, which is different from the thrust setting τ controlled by the Full-Authority Digital Engine Control (FADEC) or the pilot. The thrust lapse is plotted in Fig. 2c for the sea-level takeoff and sea-level static operating point. A second-order polynomial regression of the thrust lapse from sea-level takeoff to top-of-climb is computed from the NPSS cycle deck, i.e., $\lambda_{\mathrm{TO}} = f(M_{\mathrm{cruise}}, a, b, c)$:

$$\lambda_{\mathrm{TO}} = \frac{F_{\mathrm{n,avail.}}|_{\mathrm{TOC}}}{F_{\mathrm{n,avail.}}|_{\mathrm{TO}}} = aM_{\mathrm{cruise}}^2 + bM_{\mathrm{cruise}} + c \quad \text{with} \begin{cases} a = +0.386 \\ b = -1.022 \\ c = +0.933 \end{cases} \tag{21}$$

Furthermore, a second-order polynomial regression of the thrust lapse between top-of-climb and sea-level static, $\lambda_{\mathrm{SLS}} = f(M_{\mathrm{cruise}}, a, b, c)$, is given by

$$\lambda_{\mathrm{SLS}} = \frac{F_{\mathrm{n,avail.}}|_{\mathrm{TOC}}}{F_{\mathrm{n,avail.}}|_{\mathrm{SLS}}} = aM_{\mathrm{cruise}}^2 + bM_{\mathrm{cruise}} + c \quad \text{with} \begin{cases} a = +0.346 \\ b = -0.922 \\ c = +0.832 \end{cases} \tag{22}$$

The coefficients a, b, and c in the equations are governed by the engine design parameters.

Figure 3 shows Eq. (17) as a function of cruise Mach number for $\Lambda_{\mathrm{TO}} = 7$ and $N_e \in [2, 3, 4]$. Increasing the number of installed engines decreases the allowable cutback thrust setting as the OEI requirement becomes less stringent. Such increased thrust cutbacks enable jet velocity reduction [see Eq. (5)] and thus source noise reduction. The benefit reduces as the number of engines is increased, as it scales with $N_e/(N_e - 1)$. Furthermore, the allowable cutback thrust setting increases as the cruise Mach number increases, governed by the thrust lapse between the top-of-climb and takeoff operating point, $F_{\mathrm{n,avail.}|_{\mathrm{TOC}}}/F_{\mathrm{n,avail.}|_{\mathrm{TO}}}$, as shown in Fig. 3.

B. Flyover Propagation Distance, r_{flyover}

The operational space of takeoff trajectories for SST is explored to formulate the expression [Eq. (13)] for the flyover propagation distance as a function of the scaling groups identified in Sec. III. The takeoff trajectories are computed using the trajectory model developed by Voet et al. [17]. In this section, it is chosen to present the results in terms of the sea-level static thrust loading ψ_{SLS} rather than the cruise Mach number, as this provides a more intuitive insight into the takeoff trajectory operational space. The sea-level static thrust loading ψ_{SLS} can be written as a (decreasing) function of the cruise Mach number using $\psi_{\mathrm{SLS}} = (1/\lambda_{\mathrm{SLS}}) \cdot \psi_{\mathrm{TOC}}$. The thrust loading at top-of-climb is given by Eq. (19); the thrust lapse between top-of-climb and sea-level static, λ_{SLS}, is given by Eq. (22). Substituting the aerodynamic efficiency target by Küchemann [21], the rate of climb $V_z = 4.11\mathrm{m/s}$, and the cruise velocity $V_{\mathrm{cruise}} = 295M_{\mathrm{cruise}}$, the sea-level static thrust loading is given by

$$\psi_{\mathrm{SLS}} = \frac{1}{0.346M_{\mathrm{cruise}}^2 - 0.922M_{\mathrm{cruise}} + 0.832}\left[\frac{M_{\mathrm{cruise}}}{3(M_{\mathrm{cruise}} + 3)} + \frac{4.11}{295M_{\mathrm{cruise}}}\right] \tag{23}$$

The range of cruise Mach numbers $M_{\mathrm{cruise}} \in [1.4, 2.2]$ corresponds to a (decreasing) range of sea-level static thrust loading, $\psi_{\mathrm{SLS}} \in [0.52, 0.31]$.

First, the SST takeoff trajectory operational space is assessed by first looking at hypothetical trajectories using a set of simplifying assumptions (see Table 2), with the objective of finding a closed-form expression of the flight path (x, z) as a function of the scaling groups ψ_{SLS}, Λ_{TO}, and $V_{\mathrm{TO}}^2/x_{\mathrm{flyover}}g$. Then, the expression for the flight path is corrected when considering actual takeoff trajectories without the simplifying assumptions in Table 2. Finally, the expression for the flight path of the actual takeoff trajectories is employed to compute the flyover propagation distance as a function of the scaling groups.

1. Hypothetical Takeoff Trajectory Operational Space

The hypothetical takeoff trajectory operational space is shown in Fig. 4a. The flight path of the trajectories in the operational space covers a wide space in the (x, z) domain. In order to find a single expression for the flight path of a vehicle as a function of the scaling groups, a coordinate transformation is applied. The velocity V, acceleration a, time t, horizontal distance x, vertical distance z, and climb angle γ are normalized using the normalizing groups in Eqs. (24–29). The horizontal distance x and vertical distance z are independent state variables and therefore require different normalizing groups.

1) Velocity V is normalized by takeoff speed, given by a multiple of the stall speed, i.e., $k_{\mathrm{TO}}V_{\mathrm{stall}}$.

Table 2 Assumptions for the operational space exploration of the hypothetical and actual takeoff trajectories

Characteristic	Hypothetical takeoff trajectory	Actual takeoff trajectory
1. Atmospheric properties	Nonstratified (sea level)	Stratified
2. Aircraft takeoff aerodynamic efficiency	Constant across α	Variable, $\Lambda_{\mathrm{TO}} = f(\alpha)$
3. Engine available thrust	No thrust lapse, $F_n = F_{\mathrm{SLS}}$	Thrust lapse, $F_n = F_n(z, M)$

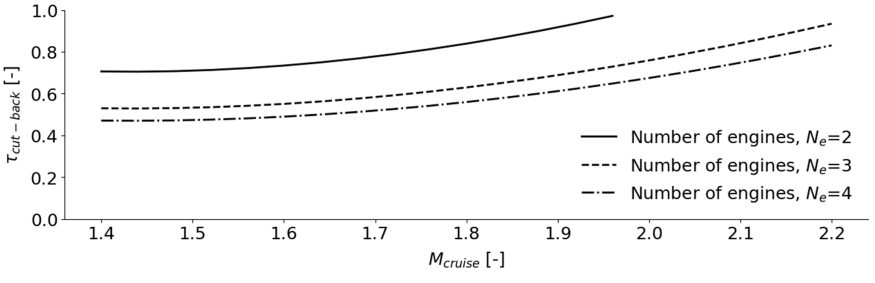

Fig. 3 Minimum allowable cutback thrust setting at takeoff, τ_{cutback}, as a function of cruise Mach number for $\Lambda_{\mathrm{TO}} = 7$ and $N_e \in [2,3,4]$.

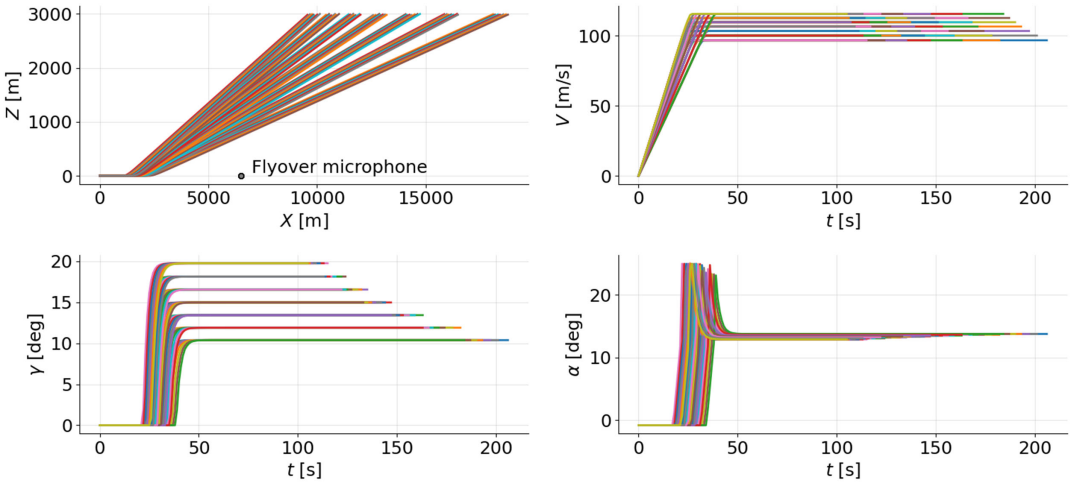

a) In physical coordinate system

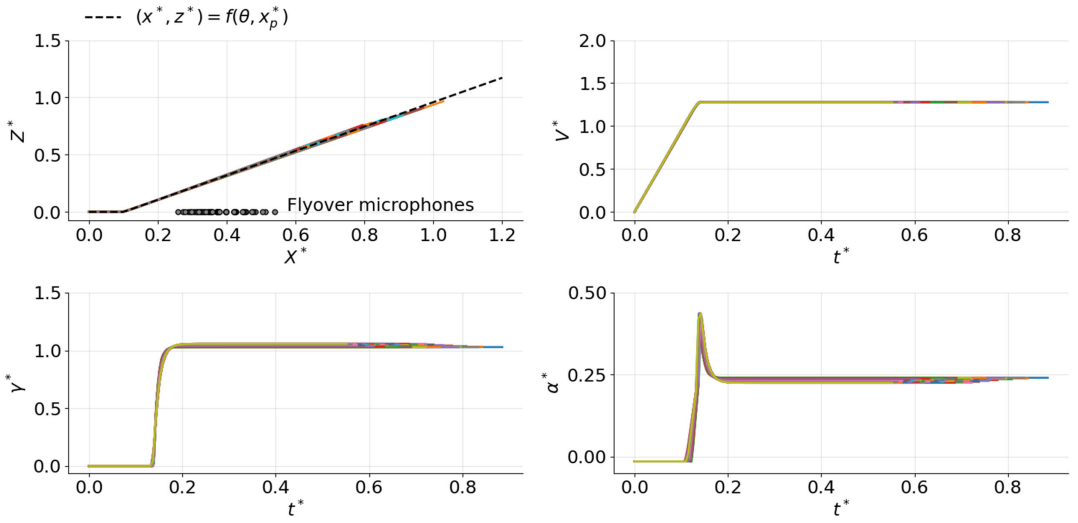

b) In normalized coordinate system

Fig. 4 Hypothetical takeoff trajectory operational space for vehicles with scaling groups $\psi_{SLS} \in [0.325 - 0.475]$, $\Lambda_{TO} = 7$, $(V_{TO}^2/x_{flyover}g) \in [0.146, 0.209]$, and $N_e = 3$.

$$V^* = V \cdot \left[\frac{1}{V_{TO}}\right] \tag{24}$$

2) Acceleration a is normalized by the sea-level static thrust loading ψ_{SLS}. Using Newton's second law, the acceleration can be rewritten as $a = (F/m) = (F/W)g = \psi_{SLS}g$.

$$a^* = a \cdot \left[\frac{1}{\psi_{SLS}g}\right] \tag{25}$$

3) Time t is normalized using the combination of Eqs. (24) and (25), i.e., $t = (v/a)$:

$$t^* = t \cdot \left[\frac{\psi_{SLS}g}{V_{TO}}\right] \tag{26}$$

4) Horizontal distance x is normalized using the combination of Eqs. (24–26), i.e., $x = v \cdot t$:

$$x^* = x \cdot \left[\frac{\psi_{SLS}g}{V_{TO}^2}\right] \tag{27}$$

5) Climb angle γ is normalized using the equation of motion along the velocity vector for steady flight at sea level, i.e., $\gamma \approx (\psi_{SLS} - (1/\Lambda_{TO}))$ [see Eq. (12)] for small angles γ. The climb angle is expressed in radians.

$$\gamma^* = \gamma \cdot \left[\frac{1}{\psi_{SLS} - \frac{1}{\Lambda_{TO}}}\right] = \gamma \cdot \left[\frac{1}{\Gamma}\right], \quad \text{where } \Gamma = \left(\psi_{SLS} - \frac{1}{\Lambda_{TO}}\right) \tag{28}$$

6) Vertical distance z is normalized using the combination of Eqs. (27) and (28), i.e., noting that $z = x \tan\gamma \approx x\gamma$ for small angles γ:

$$z^* = z \cdot \left[\frac{\psi_{SLS}g}{V_{TO}^2}\right] \cdot \left[\frac{1}{\Gamma}\right] \tag{29}$$

7) Angle of attack, α, is expressed in radians.

Figure 4b shows the takeoff trajectories; operational space in the normalized coordinate system. By applying the coordinate transformation, all takeoff trajectories collapse onto a single line for all state and control variables. Equations (24–29) transform the trajectories from the physical coordinate system (x, z) to the normalized coordinate system (x^*, z^*):

$$(x, z = f(x)) \rightarrow \left(x^*, z^* = \begin{cases} 0 & \text{if } 0 \le x^* \le x^*_{liftoff} \\ (x^* - x^*_{liftoff})\tan\gamma^* & \text{if } x^* > x^*_{liftoff} \end{cases}\right) \tag{30}$$

The two constants $\gamma^* = 0.817$ and $x^*_{liftoff} = 0.1$ are extracted from the dashed line in the (x^*, z^*) plot in Fig. 4b. These constants

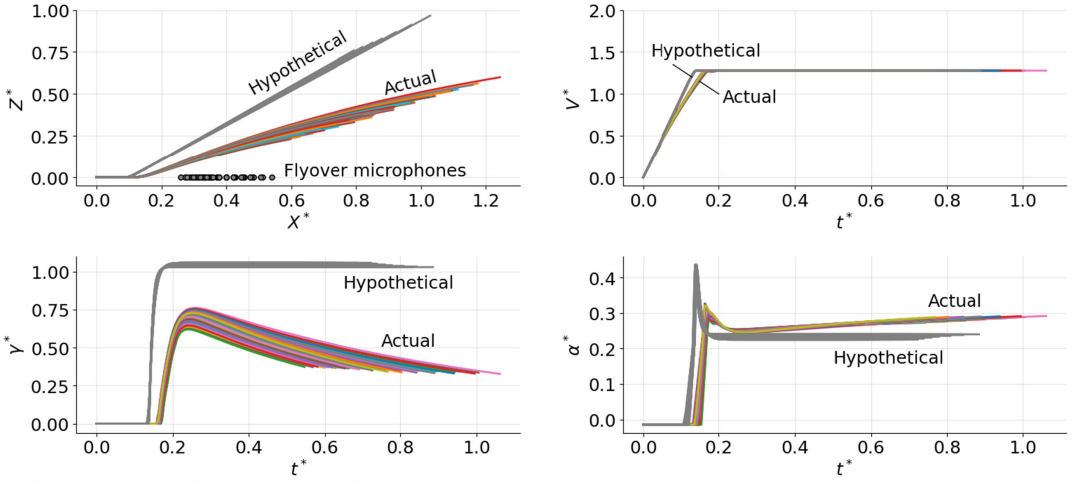

a) Hypothetical take-off trajectory operational space evaluated at: non-stratified atmosphere, constant aerodynamic efficiency ($\Lambda_{TO} = 7$), sea level static thrust, $F_n = F_{SLS}$

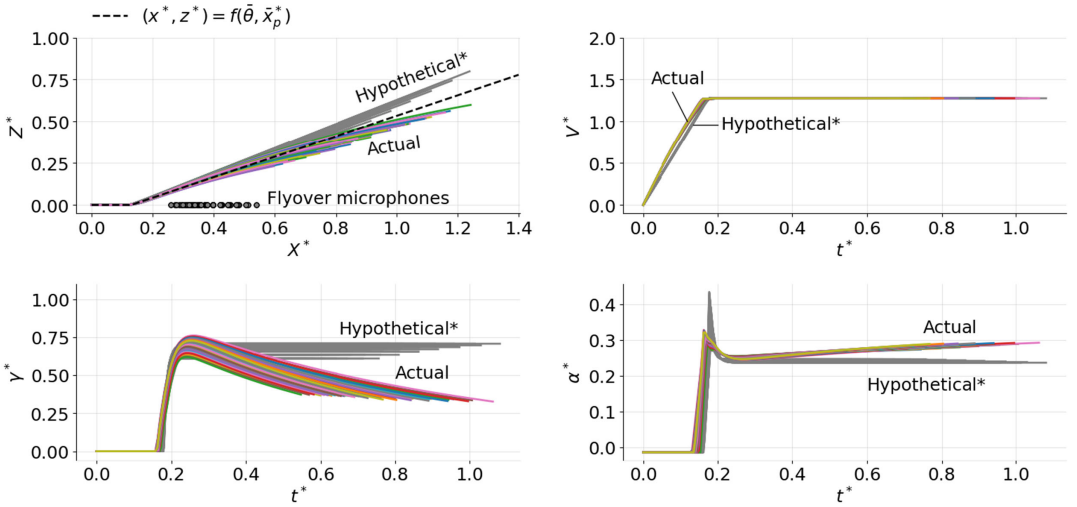

b) Hypothetical take-off trajectory operational space evaluated at: stratified atmosphere, variable aerodynamic efficiency ($\Lambda_{TO} = f(\alpha)$), average climb-out thrust, $F_n = 0.782 F_{SLS}$

Fig. 5 Comparison of actual and hypothetical takeoff trajectory operational space for vehicles with scaling groups $\psi_{SLS} \in [0.325 - 0.475]$, $\Lambda_{TO} = 7$, and $(V_{TO}^2/x_{flyover}g) \in [0.146, 0.209]$.

completely determine the trajectory operational space in the normalized coordinate system. The fixed flyover microphone in the physical coordinate system is transformed to an array of microphones in the normalized coordinate system:

$$(x = x_{\text{flyover}}, z = 0) \rightarrow \left(x^* = \left[\frac{x_{\text{flyover}} g}{V_{\text{TO}}^2}\right]\psi_{\text{SLS}} = \frac{\Pi_8}{\Pi_9}, z^* = 0\right) \tag{31}$$

The method to compute the flyover propagation distance from Eqs. (30) and (31) is presented in Sec. IV.B.3.

2. *Actual Takeoff Trajectory Operational Space*

Figure 5a shows the operational space for the actual takeoff trajectories in the normalized coordinate system. The same range of mission and vehicle parameters listed in Sec. IV.B.1 is used. The normalized hypothetical (x, z) trajectory is also included in Fig. 5a for comparison. The coordinate transformation developed in Sec. IV.B.1 is effective at collapsing the set of variables (t, x, v, α) to a single line for the actual takeoff trajectories. However, this is not the case for the vertical distance z and the climb angle γ, as z and γ fan out during the climb. The flight path (x^*, z^*) of the actual trajectories in the normalized coordinate system can still be *approximated* by a single line. However, the climb rate of the actual trajectories is approximately half the climb rate of the hypothetical trajectories. This difference is attributed to engine thrust lapse effect.

Rather than the sea-level static thrust—as for the hypothetical takeoff trajectory operational space—a better approximation of the thrust in the actual takeoff trajectory operational space is the (constant) average climb-out thrust. A *modified* hypothetical takeoff trajectory is defined using the following assumptions: stratified atmosphere, variable aerodynamic efficiency as function of angle of attack ($\Lambda = f(\alpha)$), and no engine thrust lapse. However, the net thrust is set to the average climb-out thrust instead of the sea-level static thrust, i.e., $\psi = 0.782\psi_{\text{SLS}}$.[¶] The modified hypothetical takeoff trajectory, marked with (*), is compared to the actual takeoff trajectory operational space in Fig. 5b. The modified hypothetical trajectory now closely approximates the actual takeoff trajectories. The use of the constant average climb-out thrust is incorporated in the expression for the flight path by just updating the characteristic variables γ^* and x^*_{liftoff}. The updated characteristic variables are given by $\bar{\gamma}^* = 0.54$ and $\bar{x}^*_{\text{liftoff}} = 0.13$. The updated expression for the flight path, i.e., the dashed line in Fig. 5b, is able to approximate the flyover distance of the actual trajectories within $[-15, +24]\%$.

[¶]The average thrust between the liftoff point ($z = 0$, $V = V_{\text{TO}}$) and the end of climb point ($z = 1000$ m, $V = V_{\text{TO}}$) is denoted as the average climb-out thrust.

3. Equation for the Flyover Propagation Distance

A first-of-its-kind expression is derived explicitly providing a functional form of the flyover propagation distance as a function of the relevant scaling groups identified in Sec. III:

$$\frac{r_{\text{flyover}}}{x_{\text{flyover}}} = \left(1 - \underbrace{\bar{x}^*_{\text{liftoff}} \frac{V^2_{\text{TO}}}{x_{\text{flyover}} g} \frac{1}{\psi_{\text{SLS}}}}_{\text{Phase1: Ground roll}}\right) \underbrace{\frac{\Gamma \sin \bar{\gamma}^*}{\sqrt{\Gamma^2 \sin^2 \bar{\gamma}^* + \cos^2 \bar{\gamma}^*}}}_{\text{Phase2: Climb-out}} \tag{32}$$

A detailed derivation of Eq. (32) is given in Appendix B. Equation (32) clearly shows two key terms corresponding to the two phases of the takeoff trajectory, i.e., the ground roll and the climb-out. The key trends of the flyover distance with SST mission and vehicle parameters are as follows:

1) Increasing aircraft sea-level static thrust loading results in increasing the flyover distance. An increase in sea-level static thrust loading reduces both the groundroll distance as well as the climb-out angle of the takeoff trajectory. Both of these effects result in an increase in flyover distance. Consequently, since sea-level static thrust loading is a decreasing function of cruise Mach number, the flyover distance decreases with increasing cruise Mach number.

2) Increasing the takeoff aerodynamic efficiency increases the aircraft climb angle and, thus, also the flyover distance.

3) Increasing takeoff speed increases the ground roll distance, which reduces the flyover distance. The takeoff speed can be increased by increasing aircraft wing loading, reducing the maximum lift coefficient at takeoff, as well as increasing the takeoff velocity ratio k_{TO}.

Equation (32) for the flyover propagation distance and Eqs. (15–17) for the engine source strength are substituted in Eq. (2) to obtain the full functional form of the noise level at the microphone.

C. Proportionality Coefficients of Source Strength and Propagation Effects

The coefficients c_1 and c_2 in Eq. (2) determine the proportionality between the noise source strength and propagation effects. Rather than using first principles to determine the value of the proportionality coefficients, it is opted to use high-fidelity noise data to anchor the coefficients c_1 and c_2 using a least-square estimate.

The pyNA aircraft noise estimation model [11] is used to obtain high-fidelity noise data in terms of EPNL at the flyover microphone for the actual takeoff trajectory operational space in Sec. IV.B.2. Note that this operational space does not include a thrust cutback (i.e., $\tau_{\text{cutback}} = 1$), and thus the following equation is used to obtain a least-square estimate for c_1 and c_2:

$$P_{\text{flyover}} = c_1 \cdot 80 \log_{10}(V_{j,\tau=1} - V_{\text{TO}}) + c_2 \cdot 20 \log_{10}\left(\frac{1}{r_{\text{flyover}}}\right) \tag{33}$$

The resulting least-squares fit for the proportionality constants is given by $c_1 = 0.762$ and $c_2 = 0.978$. Equation (33) is able to approximate the flyover noise levels of takeoff trajectories within $[-0.36, +0.41]$ dB of the pyNA simulations. This small error implies that the functional form of Eq. (33) has utility for estimating the aircraft noise levels at takeoff microphones.

D. Summary of Reduced-Order Model Key Assumptions

The key assumptions used in the reduced-order model are summarized below:

1) Takeoff noise levels are obtained by propagating a compact noise source strength. The source noise is governed by the jet velocity; the propagated noise is governed by the aircraft-to-microphone propagation distance.

2) SST engines are sized at mission top-of-climb as the most demanding operating point.

3) Specific thrust at the engine sizing point is only a function of cruise Mach number; changes in aircraft weight and range are counterbalanced by changes in engine mass flow and thus have no effect on engine specific thrust or on takeoff noise levels.

4) The engine thermodynamic cycle is only a function of the cruise Mach number. Thus, the relation between the takeoff and top-of-climb operating points, and consequently the engine mixed jet velocity at takeoff, are only a function of the cruise Mach number.

5) The high-speed (cruise) aerodynamic efficiency (lift-to-drag ratio) of SST is only a function of cruise Mach number.

6) The low-speed (takeoff) aerodynamic efficiency (lift-to-drag ratio) of SST scales with takeoff velocity squared.

7) The minimum allowable cutback thrust is governed by the steady level flight with one-engine-inoperative requirement.

8) The lateral microphone position in the ICAO noise certification framework is located on the sideline ($y = 450$ m) at the point where the aircraft reaches 300 m (985 ft) altitude.

9) Operational part-power takeoff procedures are not considered in this paper.

10) A hypothetical takeoff trajectory is defined for an aircraft at a constant angle of attack, using an engine without thrust lapse ($\psi = \psi_{\text{SLS}}$), in a nonstratified (sea-level) atmosphere. With those assumptions, the takeoff trajectories collapse onto a single line for all state and control variables.

11) The actual takeoff trajectory operational space is approximated by the hypothetical takeoff trajectory operational space with a constant reduced takeoff thrust (i.e., $\psi = 0.782\psi_{\text{SLS}}$).

V. Application of Reduced-Order Model to Assess SST Takeoff Noise Levels

A. Comparison of Reduced-Order Model with pyNA Noise Levels for Reference Aircraft

The utility of the reduced-order model is assessed by evaluating the takeoff noise levels for two supersonic vehicles (i.e., the NASA STCA and the GT Medium SST) and comparing them to the noise levels obtained using pyNA [11]. The NASA STCA is a 55-metric-ton, 8-passenger business jet with transatlantic range cruising at Mach 1.4. The concept vehicle was developed in service of the ICAO in order to evaluate the environmental and economic impacts of SST [18]. The GT Medium SST is a 55-passenger airliner cruising at Mach 2.2. This vehicle was developed in order to investigate the impact of aircraft and vehicle technologies on the future environmental impacts of supersonic aviation [19].

The takeoff noise levels of both aircraft are evaluated for two takeoff trajectories, i.e., the high-altitude and low-altitude single thrust cutback trajectories, as illustrated in Fig. 6. Voet et al. [17] surveyed the single thrust cutback operational space*** for the NASA STCA and identified two local minima: the high-altitude thrust cutback minimizing the noise level at the flyover microphone, and the low-altitude thrust cutback minimizing the noise level at the lateral microphone. Furthermore, they used an optimal control framework to develop automatic continuous thrust control (i.e., programmed thrust cutback) schedules to minimize the sum of lateral and flyover noise levels for the NASA STCA. They found that a thrust-setting schedule characterized by a thrust cutback followed by a thrust bump resulted in minimum takeoff noise levels. To avoid dealing with the large range of possible VNRS for SST, this work hypothesizes a trajectory resulting in a *strict lower limit* for the takeoff noise level of SST using programmed thrust cutback: the combination of the lateral noise level from the low-altitude cutback scenario and the flyover noise level from the high-altitude cutback scenario. This lower limit serves as a measure for the takeoff noise reduction potential of SST using programmed thrust cutback schedules.

The NASA STCA and GT Medium SST takeoff noise levels are estimated using the reduced-order model for the high-altitude and low-altitude single thrust cutback trajectories, resulting in minimum flyover and lateral noise levels, respectively. Figure 7 shows the

***The single thrust cutback (STCB) operational space is characterized by 2 degrees of freedom: cutback thrust level and cutback altitude.

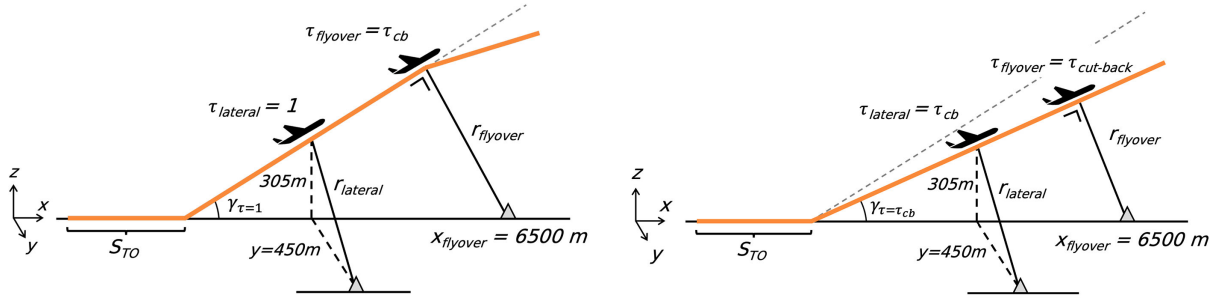

a) High-altitude thrust cut-back b) Low-altitude thrust cut-back

Fig. 6 Sketch of reference takeoff trajectories.

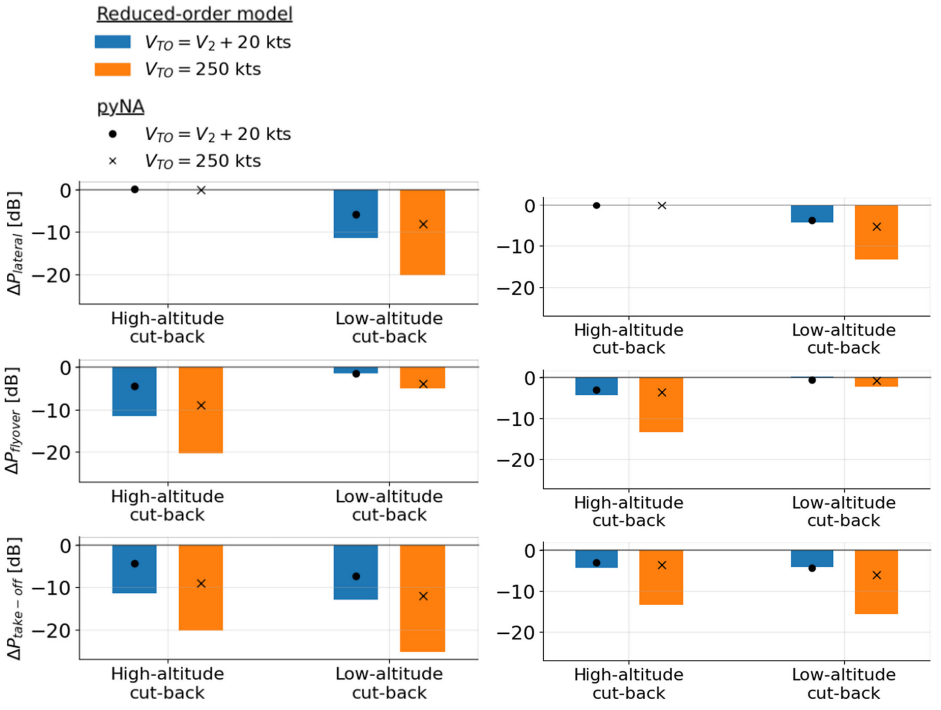

a) NASA STCA b) GT Medium SST

Fig. 7 Lateral (top), flyover (center), and takeoff (bottom) noise level reduction for high-altitude and low-altitude STCB trajectories as computed with the reduced-order model and pyNA.

difference in lateral, flyover, and takeoff noise levels between the cutback scenarios and a takeoff trajectory without cutback, as calculated using the reduced-order model and using pyNA [11]. The comparison is carried out for two takeoff speeds: a *low*-speed trajectory at $V_2 + 20$ kts and a *high*-speed trajectory at 250 kts.[†††] This assessment shows that the following trends are correctly captured by the reduced-order model:

1) The high-altitude cutback scenario does not result in any change in lateral noise. This is by definition of the high-altitude cutback, which happens downstream of the domain of dependence of the lateral microphone.

2) The noise reduction potential of the thrust cutback at both lateral and flyover microphones is less for the GT Medium SST compared to the NASA STCA.

3) The noise reduction potential for the high-speed ($V_{TO} = 250$ kts) trajectories is higher compared to the low-speed ($V_{TO} = V_2 + 20$ kts) trajectories.

Comparing the reduced-order model with the pyNA results, Fig. 7 shows that the reduced-order model overestimates the quantitative value of the thrust cutback noise reduction. It can thus be inferred that it mostly overestimates the noise reduction due to thrust cutback at the different microphones. The error in $\Delta\text{EPNL}_{\text{takeoff}}$ between the reduced-order model and the pyNA simulations can be up to 13.0 EPNdB for the NASA STCA, and up to 9.5 EPNdB for the GT Medium SST. However, the key objectives of developing the reduced-order model are to capture a) the *trends* of takeoff noise performance for vehicles designed within a range of cruise Mach numbers and b) assess the effect of key vehicle design parameters on the SST takeoff noise performance. By capturing the trends delineated in the above, the reduced-order model achieves these objectives and provides a useful tool for assessing the noise performance of a wide range of SST.

B. Takeoff Noise Assessment for a Broad Class of Supersonic Vehicles

1. *SST Takeoff Noise Scaling with Cruise Mach Number*

The takeoff noise levels for a broad class of SST vehicles are assessed using the reduced-order model for four trajectories: a) without thrust cutback, b) using high-altitude single thrust cutback, c) using low-altitude single thrust cutback, and d) using programmed thrust cutback, resulting in a lower limit for takeoff noise levels (see Sec. V.A). Figure 8 shows the takeoff noise levels for the range $M_{\text{cruise}} \in [1.4, 2.2]$, assuming a takeoff aerodynamic efficiency $\Lambda_{\text{TO}} = 7$, the number of engines, $N_e = 3$, and a takeoff speed ratio

[†††]A maximum takeoff speed of 128.6 m/s (250 kts) below 3048 m (10,000 ft) altitude is defined in the General Operating and Flight Rules (*14 CFR §91.117.a*) [25].

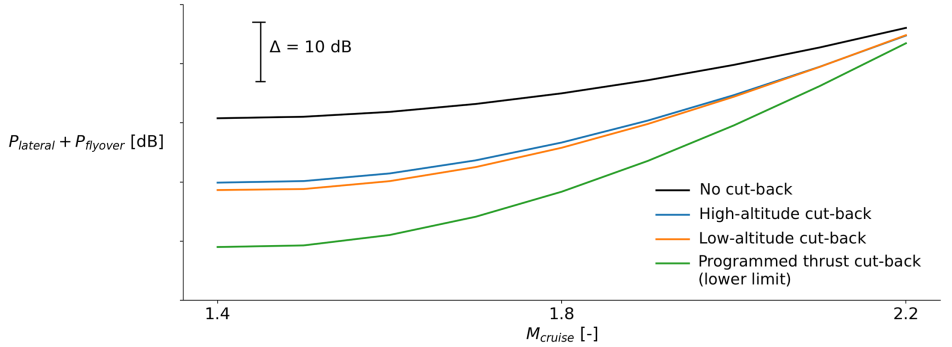

Fig. 8 SST takeoff noise levels as a function of cruise Mach number for takeoff trajectories with 4 cutback scenarios; $\Lambda_{TO} = 7$, $N_e = 3$, $(V_{TO}^2/x_{flyover}g) = 0.149$.

$(V_{TO}^2/x_{flyover}g) = 0.149$. Figure 8 highlights two trends for the SST noise levels as a function of cruise Mach number:

1) SST takeoff noise levels increase with the increasing cruise Mach number. Assuming a constant number of installed engines, wing loading, aerodynamic efficiency, and maximum lift coefficient, a Mach 2.2 aircraft is found to be ∼15.3 dB louder compared to a Mach 1.4 aircraft. This is governed by the following:

a) *Source noise* increases as a function of an increasing cruise Mach number. As shown in Fig. 2a, higher-cruise-Mach-number engines have higher specific thrust, resulting in higher mixed jet velocities.

b) *Propagated noise* increases with increasing cruise Mach numbers. As shown by Eq. (32), increasing the cruise Mach number corresponds to decreasing the sea-level static thrust loading, which reduces the flyover propagation distance.

2) The takeoff noise reduction potential of the cutback scenarios—indicated by the difference between the solid line and the dashed, dashed-dotted, and dotted lines in Fig. 8—decreases with the increasing cruise Mach number. The thrust cutback noise reduction potential of the Mach 2.2 aircraft is found to be ∼19.2 dB less compared to the Mach 1.4 aircraft. As shown in Fig. 2c, the amount of possible thrust cutback reduces, mainly governed by the reducing thrust lapse between top-of-climb and takeoff at higher cruise Mach numbers.

2. *Effect of Vehicle and Mission Scaling Groups on SST Takeoff Noise Levels*

This section assesses the effect of the vehicle and mission scaling groups on the SST takeoff noise levels for a) the high-altitude thrust cutback and b) the PTCB lower limit. The sensitivity of takeoff noise levels to changes in vehicle and mission parameters for both cutback scenarios is shown in Fig. 9. The baseline takeoff noise levels are shown in Fig. 8.

The number of installed engines, N_e, and the takeoff aerodynamic efficiency Λ_{TO} are the most effective at reducing the takeoff noise levels for both cutback scenarios. An increase in the number of installed engines enables reduced cutback thrust settings since steady-level flight with OEI becomes less stringent. This results in reduced source noise at both the lateral and the flyover microphones. As shown in Eq. (32), increasing the takeoff aerodynamic efficiency increases the flyover propagation distance because of an increase in climb-out angle.

VI. Conclusions

The reduced-order model presented in this paper enables a physics-based assessment of the scaling of SST takeoff noise levels with cruise Mach number. As such, it can potentially yield a simple guideline for regulatory authorities to estimate approximate noise limits for SST depending on their cruise Mach number. It is found that SST takeoff noise levels, defined as the sum of lateral and flyover noise, increase with increasing cruise Mach numbers. Higher specific thrust engines and reduced sea-level static thrust loading at higher cruise Mach numbers result in an increase in source and propagated noise, respectively. Assuming constant aerodynamic efficiency, takeoff speed, and number of installed engines, the reduced-order model shows that a Mach 2.2 aircraft is ∼15.3 dB louder compared to a Mach 1.4 aircraft. Furthermore, it is found that the noise reduction potential of thrust cutback maneuvers reduces as cruise Mach number increases, which is governed by the reduced thrust lapse between top-of-climb and takeoff for high Mach number engines. The reduced-order model shows that the thrust cutback noise reduction potential of the Mach 2.2 aircraft is ∼19.2 dB less compared to the Mach 1.4 aircraft. Finally, the reduced-order model enables the sensitivity assessment of supersonic takeoff noise levels with key vehicle and mission scaling groups. The number of installed engines and takeoff aerodynamic efficiency are shown to be the key drivers for reducing takeoff noise levels for SST.

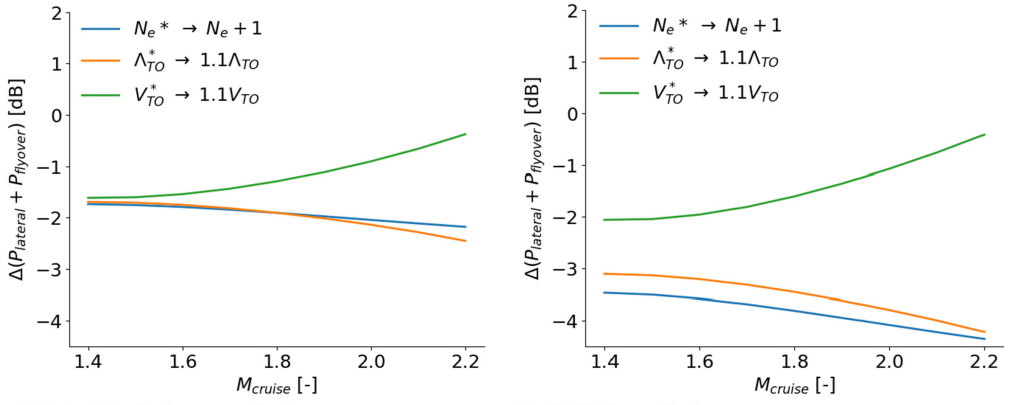

Fig. 9 Change in takeoff noise levels for changes in SST vehicle and mission parameters; baseline parameters: $\Lambda_{TO} = 7$, $N_e = 3$, and $(V_{TO}^2/x_{flyover}g) = 0.149$.

While the above constitutes a first-of-its-kind reduced-order model for the SST takeoff noise performance, further refinements for quantitative improvements are necessary. Suggested improvements include a dynamic scaling approach for the engine noise source strength as a function of key engine design parameters and an uncertainty quantification study of the key assumptions in the reduced-order model.

Appendix A: Thermodynamic Cycle Deck for SST Engines

A clean-sheet engine thermodynamics cycle deck is developed for SST with a cruise Mach number within the range $M_{\text{cruise}} \in [1.4, 2.2]$ using the NPSS software [8]. A conventional engine architecture is selected for the clean-sheet engine. The low-pressure spool of the engine consists of a fan powered by a low-pressure turbine (LPT); its high-pressure spool consists of a compressor powered by a high-pressure turbine (HPT). The core and bypass stream of the engine are fully mixed and exhausted through a variable-area converging–diverging nozzle. An external compression supersonic inlet is mounted upstream of the fan. The turbomachinery components in the clean-sheet engine are designed assuming a CFM56-5B3 technology level by assuming similar polytropic efficiency values and temperature limits. Unlike Concorde, the engines do *not* use afterburners. While afterburners enable increased net thrust at takeoff, they significantly increase thrust-specific fuel consumption and engine emissions, as well as introduce additional noise sources such as shock-cell noise. Details on the engine architecture and numerical modeling of the engine performance are presented in Prashanth et al. [26]. The performance characteristics of the NPSS engine design space sweep are computed at four operating conditions:

1) *Top-of-climb (TOC)*: Engine sizing point at $M = M_{\text{cruise}}$, $z = z_{\text{cruise}}$, and with potential rate of climb, $V_z = 4.11$ m/s.

2) *Cruise (CR)*: Steady level flight at $M = M_{\text{cruise}}$ and $z = z_{\text{cruise}}$.

3) *Sea-level takeoff (TO)*: At $M = 0.25$ and $z = 0$ and 100% fan rotational speed. This condition is used for the takeoff noise assessments.

4) *Sea-level static (SLS)*: At $M = 0$ and $z = 0$ and 100% fan rotational speed.

Figure A1 shows the compressor discharge temperature $T_{t,3}$, turbine inlet temperature $T_{t,41}$, engine overall pressure ratio OPR, and fan percent design speed $N_{\text{fan}}/N_{\text{fan,des.}}$ across the range of cruise Mach numbers for the four operating points. The engine design variables, including the pressure ratio of the fan, π_{fan}, the pressure ratio of the high-pressure compressor, π_c, as well as temperature ratio $T_{t,41}/T_{t2}$, are set to meet the following constraints:

1) The engine is sized to meet the top-of-climb thrust requirement, given by

$$\frac{F_{\text{n,req.}}}{W}\Big|_{\text{TOC}} = \left[\frac{1}{\Lambda_{\text{TOC}}} + \frac{V_z}{V_{\text{cruise}}}\right] \tag{A1}$$

2) The fan pressure $\pi_{\text{fan}} = 2$ is selected to keep the propulsive nozzle on the cusp of choke during takeoff operations, assuming a mixer extraction ratio $\text{ER}_{\text{mix}} \approx 1$. The mixed jet is kept below supersonic speeds during takeoff operations to avoid shock cell noise. A pressure ratio $\pi = (1 + (\gamma + 1)/2)^{\gamma/(\gamma-1)} = 1.89$ is required for sonic flow. Assuming a loss of 5% in the fan and mixer ducts allows for a fan pressure ratio of $\pi_{\text{fan}} \approx 2$.

3) An engine overall pressure ratio $\text{OPR} = \pi_{\text{ram}}\pi_{\text{fan}}\pi_{\text{hpc}} = 65$ (based on the NASA STCA [18]) is assumed across the range of cruise Mach numbers to limit the compressor discharge pressure and temperature, and the resulting NO_x emissions. As the ram pressure ratio increases with the increasing cruise Mach number, and the (high-pressure) compressor pressure ratio is chosen to be inversely proportional to the ram pressure ratio, i.e., $\pi_{\text{hpc}} = (\text{OPR}/\pi_{\text{fan}}\pi_{\text{ram}}) = f(M_{\text{cruise}})$.

4) A turbine inlet temperature limit, $T_{t,41} = 2000$ K, is assumed as a material limit.

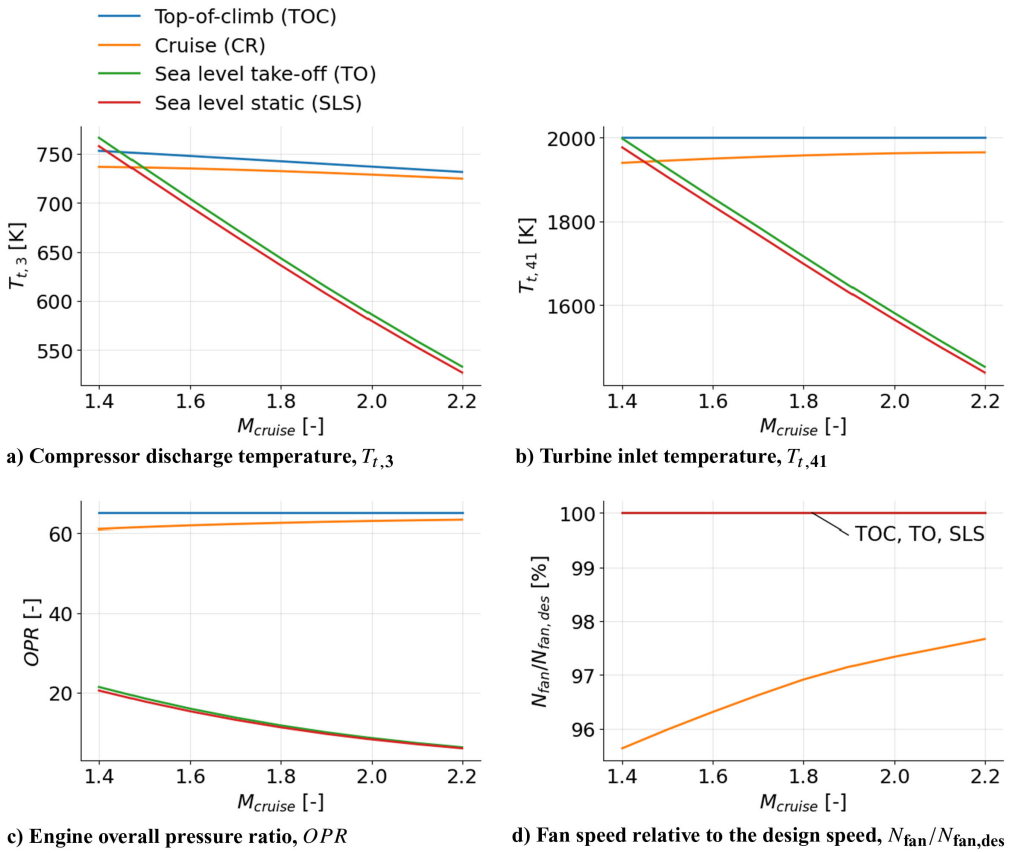

a) Compressor discharge temperature, $T_{t,3}$

b) Turbine inlet temperature, $T_{t,41}$

c) Engine overall pressure ratio, OPR

d) Fan speed relative to the design speed, $N_{\text{fan}}/N_{\text{fan,des}}$

Fig. A1 Engine characteristics across the range of cruise Mach numbers, $M_{\text{cruise}} \in$ [1.4,2.2] at the top-of-climb, cruise, sea-level takeoff, and sea-level static operating points.

The engine thermodynamic cycle deck is used to determine the scaling of the engine source terms: $V_{j,\tau=1}$, $(\partial V_j/\partial\tau)$, and τ_{cb}, as outlined in Sec. IV.A.

Appendix B: Derivation of propagation distance between SST takeoff trajectories and the flyover certification microphone

Figures B1a and B1b show sketches of the takeoff trajectory in the physical and normalized coordinate system, respectively, as introduced in Sec. IV.B.1. The coordinate normalization for the x and z coordinates is given by

$$x^* = Ax = \left[\frac{\psi_{\text{SLS}} g}{V_{\text{TO}}^2}\right] x \quad \text{and} \quad z^* = Bz = \left[\frac{\psi_{\text{SLS}} g}{V_{\text{TO}}^2}\frac{1}{\Gamma}\right] z \tag{B1}$$

where Γ is given by Eq. (28). The flyover propagation distance is computed in the physical coordinate system using

$$r_{\text{flyover}} = \sqrt{(x_{\text{flyover}} - x_S)^2 + z_S^2} \tag{B2}$$

The coordinates of point $S = (x_S, z_S)$—the point on the flight path closest to the flyover microphone—can be found by solving the following set of equations:

$$\begin{cases} \overline{SP} \cdot \overline{SR} = 0 & \text{in physical coordinate system} \\ \overline{S^*P^*} \cdot \overline{P^*R^*} = \cos\bar{\gamma}^* & \text{in normalized coordinate system} \end{cases} \tag{B3}$$

which can be rewritten as

$$\begin{cases} x_S^2 - x_{\text{liftoff}} x_S - x_{\text{flyover}} x_S + x_{\text{liftoff}} x_{\text{flyover}} + z_S^2 = 0 & \text{in the physical coordinate system} \\ A(x_S - x_{\text{liftoff}}) = \cos\bar{\gamma}^* \sqrt{A^2 (x_S - x_{\text{liftoff}})^2 + B^2 z_S^2} & \text{in then ormalized coordinate system} \end{cases} \tag{B4}$$

B.1. Case 1: High-Altitude Cutback

The system of Eq. (B4) has three solutions:

$$x_S = \begin{cases} \frac{x_{\text{flyover}} B^2 \cos^2\bar{\gamma}^* + x_{\text{liftoff}} A^2 \sin^2\bar{\gamma}^*}{B^2\cos^2\bar{\gamma}^* + A^2\sin^2\bar{\gamma}^*} \\ \frac{x_{\text{flyover}} B^2 \cos^2\bar{\gamma}^* + x_{\text{liftoff}} A^2 \sin^2\bar{\gamma}^*}{B^2\cos^2\bar{\gamma}^* + A^2\sin^2\bar{\gamma}^*} \\ x_{\text{liftoff}} \end{cases}$$

$$z_S = \begin{cases} + \frac{AB\sin\bar{\gamma}^*\cos\bar{\gamma}^*(x_{\text{liftoff}} - x_{\text{flyover}})}{B^2\cos^2\bar{\gamma}^* + A^2\sin^2\bar{\gamma}^*} \\ - \frac{AB\sin\bar{\gamma}^*\cos\bar{\gamma}^*(x_{\text{liftoff}} - x_{\text{flyover}})}{B^2\cos^2\bar{\gamma}^* + A^2\sin^2\bar{\gamma}^*} \\ 0 \end{cases} \tag{B5}$$

The third solution in Eq. (B5) is trivial; i.e., point S coincides with point P (see Fig. B1). The two other solutions are symmetric around the x axis, resulting in the same flyover distance. The liftoff distance is rewritten as $x_{\text{liftoff}} = (\bar{x}^*_{\text{liftoff}}/A)$. The angle $\bar{\gamma}^*$ and the distance $\bar{x}^*_{\text{liftoff}}$ are constants in the normalized coordinate system. The expression for the flyover distance becomes

$$\frac{r_{\text{flyover}}}{x_{\text{flyover}}} = \left(1 - \frac{\bar{x}^*_{\text{liftoff}}}{A x_{\text{flyover}}}\right) \frac{\frac{A}{B}\sin\bar{\gamma}^*}{\sqrt{\frac{A^2}{B^2}\sin^2\bar{\gamma}^* + \cos^2\bar{\gamma}^*}} \tag{B6}$$

B.2. Case 2: Low-Altitude Cutback

The normalization factor for the climb angle γ is given by

$$\gamma^* = \gamma \cdot \left[\frac{1}{\psi_{\text{SLS}} - \frac{1}{\Lambda_{\text{TO}}}}\right] \tag{B7}$$

For takeoff trajectories at constant thrust F_{SLS}, the normalized climb angle $\gamma^* = 1$. The normalized climb angle after a cutback is given by

$$\gamma^*_{\text{cutback}} = \gamma^* \frac{\left[\psi_{\text{SLS}} - \frac{1}{\Lambda_{\text{TO}}}\right]}{\left[\tau_{\text{cutback}}\psi_{\text{SLS}} - \frac{1}{\Lambda_{\text{TO}}}\right]} \tag{B8}$$

The expression in Eq. (B8) is substituted in Eq. (B6) for low-altitude cutback trajectories.

Acknowledgments

This research was funded by the U.S. Federal Aviation Administration (FAA) Office of Environment and Energy through ASCENT, the FAA Center of Excellence for Alternative Jet Fuels and the Environment, project 47 through FAA Award Number 13-C-AJFE-MIT, under the supervision of László Windhoffer and Ralph Iovinelli. Any opinions, findings, conclusions, or recommendations expressed in this material are those of the authors and do not necessarily reflect the views of the FAA. The authors would like to thank Jimmy Tai at Georgia Institute of Technology (GT) for sharing the vehicle performance data of the 55-passenger GT Medium SST as part of the FAA ASCENT10 project.

References

[1] Rutherford, D., Graver, B., and Chen, C., "Noise and Climate Impacts of an Unconstrained Commercial Supersonic Network," The International Council on Clean Transportation, 2019, https://theicct.org/sites/default/files/publications/Supersonic_Impact_Working_Paper_20190130.pdf [retrieved 6 June 2022].

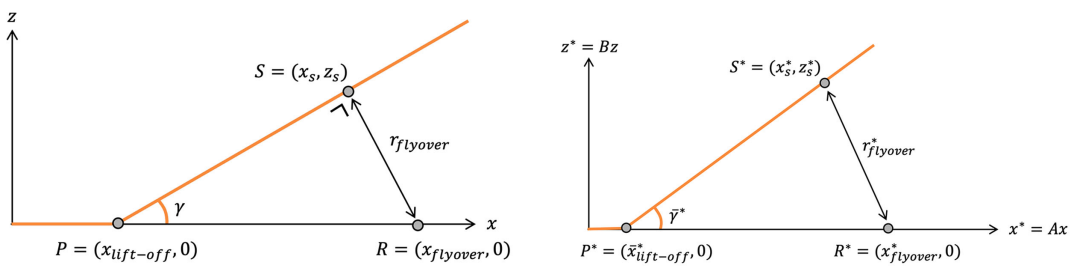

a) Physical coordinate system b) Normalized coordinate system

Fig. B1 Comparison of takeoff trajectory in physical and normalized coordinate system.

[2] "EASA Certification Noise Levels (Data Base)," European Union Aviation Safety Agency, 2021, https://www.easa.europa.eu/domains/environment/easa-certification-noise-levels#group-easa-downloads [retrieved 23 Aug. 2021].

[3] "Annex 16 to the Convention on International Civil Aviation Environmental Protection Volume 1: Aircraft Noise (Edition 8)," International Civil Aviation Organization, Montreal, Canada, 2017.

[4] "Notice for Proposed Rule Making: Noise Certification for Supersonic Airplanes (Docket No.:FAA-2020-0316; Notice No. 20-60)," Federal Aviation Administration TR-71, Washington, D.C., 2020, https://www.federalregister.gov/documents/2020/04/13/2020-07039/noise-certification-of-supersonic-airplanes [retrieved 6 June 2022].

[5] "Advance Notice of Proposed Amendment 2022-05: Environmental Protection Requirements for Supersonic Transport Aeroplanes," European Union Aviation Safety Agency (EASA), RMT.0733, Cologne, Germany, 2022, https://www.easa.europa.eu/en/document-library/notices-of-proposed-amendment/npa-2022-05#group-easa-downloads [retrieved 22 Feb. 2023].

[6] "Views of the United States on Supersonic Aircraft Noise Future Work during the CAEP/13 Cycle," Committee on Aviation Environmental Protection (CAEP), 2022, https://icao.usmission.gov/wp-content/uploads/sites/280/CAEP.12.WP_.064.16.en-VIEWS-OF-THE-UNITED-STATES-ON-SUPERSONIC-AIRCRAFT-NOISE-FUTURE-WORK-DURING-THE-CAEP13-CYCLE.pdf [retrieved 25 June 2023].

[7] Bridges, J. E., Stephens, D., and Berton, J. J., "Quantifying Uncertainty of Landing and Takeoff Noise for Commercial Supersonic Aircraft," *28th AIAA/CEAS Aeroacoustics 2022 Conference*, AIAA Paper 2022-3051, 2022. https://doi.org/10.2514/6.2022-3051

[8] Claus, R. W., Evans, A. L., Lylte, J. K., and Nichols, L. D., "Numerical Propulsion System Simulation," *Computing Systems in Engineering*, Vol. 2, No. 4, 1991, pp. 357–364. https://doi.org/10.1016/0956-0521(91)90003-N

[9] Falck, R. D., Gray, J. S., Ponnapalli, K., and Wright, T., "dymos: A Python Package for Optimal Control of Multidisciplinary Systems," *Journal of Open Source Software*, Vol. 6, No. 59, 2021, Paper 2809. https://doi.org/10.21105/joss.02809

[10] Gray, J. S., Hwang, J. T., Martins, J. R., Moore, K. T., and Naylor, B. A., "OpenMDAO: An Open Source Framework for Multidisciplinary Analysis and Optimization," *Structural and Multidisciplinary Optimization*, Vol. 59, No. 4, 2019, pp. 1075–1104. https://doi.org/10.1007/s00158-019-02211-z

[11] Voet, L. J. A., Prashanth, P., Speth, R. L., Sabnis, J. S., Tan, C. S., and Barrett, S. R. H., "Sensitivities of Aircraft Acoustic Metrics to Engine Design Variables for Multidisciplinary Optimization," *AIAA Journal*, Vol. 60, No. 8, 2022, pp. 4764–4774. https://doi.org/10.2514/1.J061411

[12] Berton, J. J., Jones, S. M., Seidel, J. A., and Huff, D. L., "Noise Predictions for a Supersonic Business Jet Using Advanced TakeOff Procedures," *Aeronautical Journal*, Vol. 122, No. 1250, 2018, pp. 556–571. https://doi.org/10.1017/aer.2018.6

[13] Kharina, A., Macdonald, T., and Rutherford, D., "Environmental Performance of Emerging Supersonic Transport Aircraft," The International Council on Clean Transportation, 2018, https://theicct.org/wp-content/uploads/2021/06/Environmental_Supersonic_Aircraft_20180717.pdf [retrieved 6 June 2022].

[14] Henne, P. A., "Case for Small Supersonic Civil Aircraft," *Journal of Aircraft*, Vol. 42, No. 3, 2005, pp. 765–774. https://doi.org/10.2514/1.5119

[15] "Environmental Technical Manual, Vol. I, Procedures for the Noise Certification of Aircraft. Document 9501; 2nd Edition," ICAO TR-9501 AN/929, Committee on Aviation Environmental Protection (CAEP), Montreal, Canada, 2015, https://www.icao.int/environmental-protection/Documents/SGAR.2015.ETM.Vol.1.pdf [retrieved 17 June 2023].

[16] "High-Speed Civil Transport Study," Boeing Commercial Airplanes, NASA CR-4233, Seattle, WA, 1990, https://ntrs.nasa.gov/citations/19890018277 [retrieved 11 May 2022].

[17] Voet, L. J. A., Prashanth, P., Speth, R. L., Sabnis, J. S., Tan, C. S., and Barrett, S. R. H., "Automatic Continuous Thrust Control for Supersonic Transport Takeoff Noise Reduction," *Journal of Aircraft*, Vol. 61, No. 1, Nov. 2023, pp. 291–306. https://doi.org/10.2514/1.C037394

[18] Berton, J. J., Huff, D. L., Seidel, J. A., and Geiselhart, K. A., "Supersonic Technology Concept Aeroplanes for Environmental Studies," *AIAA Scitech 2020 Forum*, AIAA Paper 2020-0263, 2020. https://doi.org/10.2514/6.2020-0263

[19] Mavris, D., Tai, J., Dussauge, T., Da Silva Oliveira, T., Ougazzaden, N., Fazzini, T., Hong, R., Iyengar, N., Sampaio, B., Tran, K., et al., "ASCENT Project 10 Aircraft Technology Modeling and Assessment; Georgia Tech Medium SST 55-pax Version 11.5. Data Obtained Through Personal Communication Through FAA Funded Project," 2020, https://ascent.aero/project/aircraft-technology-modeling-and-assessment/ [retrieved 19 Nov. 2020].

[20] Lighthill, M. J., "On Sound Generated Aerodynamically I. General Theory," *Proceedings of the Royal Society of London. Series A. Mathematical and Physical Sciences*, Vol. 211, No. 1107, 1952, pp. 564–587. https://doi.org/10.1098/rspa.1952.0060

[21] Küchemann, D., *The Aerodynamic Design of Aircraft*, AIAA, Reston, VA, 2012, pp. 338–342.

[22] "Title 14: Aeronautics and Space—§B36.3: Reference Noise Measurement Points," Code of Federal Regulations, 2022, https://www.ecfr.gov/current/title-14/chapter-I/subchapter-C/part-36/appendix-Appendix%20B%20to%20Part%2036 [retrieved 29 July 2023].

[23] Olson, E. D., "Advanced Takeoff Procedures for High-Speed Civil Transport Community Noise Reduction," *SAE Technical Papers*, Vol. 1, Jan. 1992, pp. 1612–1625. https://doi.org/10.4271/921939

[24] Nicolai, L. M., and Carichner, G. E., *Fundamentals of Aircraft and Airship Design*, AIAA, Reston, VA, 2010, pp. 126–127.

[25] "Title 14: Aeronautics and Space—§91.117.a: Aircraft Speed," Code of Federal Regulations, 2022, https://www.ecfr.gov/current/title-14/chapter-I/subchapter-F/part-91/subpart-B/subject-group-ECFRe4c59b5f5506932/section-91.117# [retrieved 28 June 2023].

[26] Prashanth, P., Voet, L. J. A., Speth, R. L., Sabnis, J. S., Tan, C. S., and Barrett, S. R. H., "Impact of Design Constraints on Noise and Emissions of Derivative Supersonic Engines," *Journal of Propulsion and Power*, Vol. 39, No. 3, 2023, pp. 454–463. https://doi.org/10.2514/1.B38918